Research Article

Urban heat island amplification estimates on global warming using an albedo model

Alec Feinberg[1]

Received: 14 May 2020 / Accepted: 12 November 2020 / Published online: 11 December 2020

Abstract
In this paper, we provide nominal and worst-case estimates of radiative forcing due to the UHI effect using a Weighted Amplification Albedo Solar Urbanization model. This calculation is done with the help of reported findings from UHI footprint and heat dome studies that simplify estimates for UHI amplification factors. Using this method, we quantify a global warming range due to the UHI effect, including its extent. Forcing estimates varied approximately between 0.07 and 0.87 W/m^2 representing 3% to 36% of global warming relative to the greenhouse gas forcing estimates between 1950 and 2019. Variations in our model are due to the urbanized area and associated UHI amplification estimate uncertainties. However, the model showed consistent values of about 0.16 W/m^2/% solar effective amplified areas and 1.6 W/m^2/%Δalbedo for the urbanized coverage forcing values. The basic model is additionally used to quantify feedback warming due to Arctic sea ice loss. Feedback estimates contribute to the impact of UHI forcing assessments. From our median estimates, it is concluded that UHIs contribute significantly to global warming trends. The model is versatile and also provides UHI albedo reverse forcing assessments. The results provide insight into the UHI area effects from a new perspective using a global view albedo model compared to prior ground-based measurement studies. It also illustrates the utility of using effective UHI amplification estimates when assessing their warming effect on a global scale.

Keywords Urban heat islands · Albedo modeling · UHI amplification effects · UHI heat dome · Cool roofs · Sea ice warming

1 Introduction

There are few recent publications about possible UHI influences on global warming. Thus, more up-to-date related studies, including UHI amplification effects that will be discussed in this paper, could offer supporting data for climate change theories and solutions.

One key paper often referred to is by McKitrick and Michael's [1, 2], who found in 2004 and 2007 using regression trends on socioeconomic, geographical, and temperature indicators that the net warming bias at the global level may explain as much as half the observed land-based warming. Another independent study often quoted by De Laat and Maurellis [3] in 2006 found very similar results. In 2007, IPCC [4] questioned these findings stating "the locations of greatest socioeconomic development are also those that have been most warmed by atmospheric circulation changes, which exhibit large-scale coherence." Therefore, inferring that correlation to warming was not statistically significant but a result of atmospheric oscillations. In 2009, Schmidt [5] agreed and published a paper also suggesting that McKitrick and Michael's observed correlations were probably spurious. However, in 2010, McKitrick responded with two publications, the first [6] entitled, "Atmospheric Oscillations do not Explain the Temperature-Industrialization Correlation." The second by McKitrick et al. in 2010 [7] detailed that "evidence for contamination of climatic data is robust across numerous

---

✉ Alec Feinberg, dfrsoft@gmail.com | [1]DfRSoft Research, Raleigh, USA.

SN Applied Sciences (2020) 2:2178 | https://doi.org/10.1007/s42452-020-03889-3

data sets…Consequently, we conclude that important data products used for the analysis of climate change over global land surfaces may be contaminated with socioeconomic patterns related to urbanization and other socioeconomic processes." In 2013, the IPCC summarized the controversy saying [8], "it is indisputable that UHI and land-use/land-cover are real influences on raw temperature measurements. At question is the extent to which they remain in the global products." Citations and discussions in the IPCC report suggested the UHI effect would not be more than 10% of observed warming.

However, other authors have also found UHI significance [9–17]. For example, Zhao and Huang et al. [14, 16] found that UHIs contributed to warming in China by about 30%. Bian et al. [17] in China at a Shijiazhuang station for periods 1965–2012 found the urban–rural land surface temperatures (LST) trends correlated 100% to urbanization contributions, indicating the yearly increase in annual mean LST at the urban station is entirely caused by urbanization. They concluded the true impact of rising atmospheric CO_2 on the global climate may well be vastly overstated. These studies used land-based temperature station data to make assessments. To date, one can conclude that all such studies and findings were not persuasive enough to be influential in the 2015 Paris Climate Accord [18] regarding the need for UHI albedo controls as part of the worldwide effort to mitigate global warming.

This paper provides insight into these controversial findings [1–3, 6, 7, 9–17] with a WAASU model applied to two time periods, 1950 and 2019. There are currently no papers on the influence of urbanization on climate change using albedo modeling. However, this paper is restricted to UHI and its extent and does not take into account all forms of human land contamination (roads, rural human habitation, deforestation, evapotranspiration loss, anthropogenic heat release, etc.) of which should be roughly correlated in McKitrick and Michael's socioeconomic - geographical pattern analysis. In this respect, our results are likely conservative.

The WAASU model has advantages as it works from a global view rather than with ground-based studies. There are no concerns about warming oscillations or GHG interference. The model is non-probabilistic and in line with typical energy budgets (IPCC, Hartmann et al. [8]). The model uses only two key parameters: normalized solar effective amplified area and weighted albedo values. Because it is simplistic, it has transparency compared with the complex land-based studies. We also show its utility by extending it to a weighted albedo solar (WAS) model for global warming estimates due to arctic ice melting in Appendix 4.

The contention that UHI effects are primarily of local significance is most likely related to urban area estimates. For example, the IPCC (Satterthwaite et al. [19]) AR5 report references a Schneider et al. [20] study that resulted in urban coverage of 0.148% of the Earth (Table 1). This seemingly small area tends to dismiss the role that the UHI effect can play in large-scale global warming. Furthermore, estimates of how much land has been urbanized vary widely in the literature, in part due to the definition of what is urban and the datasets used. Although such estimates are important for environmental studies, obtaining true estimates for the small urbanized area relative to the total land is very difficult. Compounded by the fact that there is a significant difference in how groups define the term "urban," Table 1 illustrates several variations from selected papers of interest. Also, global warming UHI amplification effects have not been quantified to a large degree related to area estimates. Urbanized average solar areas remain unknown.

In our study, one key paper listed in Table 1 is that due to Schneider et al. [20] since it is cited by the AR5 2014 IPCC report (Satterthwaite et al. [14]). In Schneider's paper, the larger area found in the GRUMP [21] study (Table 1) is criticized. Nevertheless, we incorporate the GRUMP area as an upper bound for urbanization. We note that UHI effects have been shown to arise even at very low levels of populations, i.e., towns with fewer than 10,000 people as noted by Karl et al. [25] and Chagnon [26]. The GRUMP study describes datasets with populations greater than 5,000 people while in the Schneider paper population estimates were not included. The GRUMP study combines population statistics and nightlights where the Schneider paper uses a high resolution of illuminated satellite data with decision tree algorithms. The Schneider paper appears to be focused mainly on the "built-up" urbanized area while the GRUMP study "urbanized area" (see the conclusion).

Table 1 Urbanization area extent estimates from various sources

Percent of land	Percent of Earth	References
2.7	0.783	Global Rural Urban Mapping Project (GRUMP) [21] —using NASA satellite light studies based on 2004 data and with census data
1	0.29	NASA [22], Galka [23] —from satellite data
0.51	0.148	Schneider et al. [20] —based on 2000-2001 data and referenced in the IPCC report (Satterthwaite, [19])
0.5	0.145	Zhou [24] —based on a 2000 dataset

Further clarification and guidance is provided in our conclusion where GW estimates are weighted heavily based on Schneider's value.

Therefore, we use both the Schneider et al. and GRUMP studies for the minimum nominal and maximum worst-case urbanization area estimates, respectively, and provide a weighting method for the final results. Furthermore, these area estimates were done using datasets near the year 2000, a reasonable point in time to extrapolate down to 1950 and up to 2019 (see Sect. 2.5), the two periods of this study.

1.1 UHI amplification effects

Table 2 lists key global warming causes and amplification effects. In general, the complex UHI amplification effects are responsible for the local thermal and related UHI global warming forcing issues. Propagating UHI global warming could further escalate the Earth's climate feedback response [27–29] (see the conclusion). A summary is provided in Appendix 2 of the key UHI effects listed in the table. As well, the conclusions and Appendix 2 includes a discussion on how UHI effects can contribute to climate change issues.

2 Data and methods

The Earth's solar area has physically grown since 1950 because tall UHI building side area increases. The actual growth in UHI heat intensity though incorporates all solar factors described in Table 2. Besides the tall building solar sides, as shown in the table, many solar effects create a large amplified heat issue. This is a nonlinear problem that could be perhaps impossible to model and is likely best measured instead with what is called the UHI "Footprint" (FP) area, for example. In the discussion below, authors have found that the FP correlates to UHI actual area. Therefore in this section, we expand upon the FP concept. The FP was defined as the continuous extent emanating outward from urban centers to rural areas that have evident UHI effect (i.e., ΔT was statistically larger than zero).

2.1 UHI area amplification effect

We are interested in assessing what we term the UHI complex solar amplification factor. This will only be applied to the UHI component in the WAASU model as an additional weighting factor. To determine this factor, it is logical as we discussed to first look at UHI FP studies as they provide a measure of the UHI amplified heat intensity. Zhang et al. [30] found the ecological FP of the urban land cover extends beyond the perimeter of urban areas, and the FP of urban climates on vegetation phenology they found was 2.4 times the size of the actual urban land cover. In a more recent study by Zhou et al. [31], day-night cycle temperature difference measurements were taken in China. In this study, they found the UHI effect decayed exponentially toward rural areas for the majority of the 32 Chinese cities. Their comprehensive study spanned from 2003 to 2012. They describe China as an ideal area to study since it has experienced the most rapid urbanization in the world in the decade they evaluated. They found that the FP of the UHI effect, including urban areas, was 2.3 and 3.9 times that of urban size for the day and night, respectively. We note that the average day-night amplification footprint coverage factor is 3.1.

To provide some assessment of how the UHI amplification factor scales, we note that Zhou et al. [31] found the FP physical area (km^2), correlated tightly and positively with the actual urban area having a correlation coefficient higher than 79% over 32 cities. This correlation suggests that area can be used to provide an initial estimate of this complex amplification factor. Furthermore, the fact that the amplification factor scales with the area are consistent in the calculation of the WAASU model that is weighted by area. This is discussed in Appendix 1 and Sect. 2.5 (Eq. 9).

Therefore, as a model assumption, it is reasonably justified that the amplification factor (AF) should scale with the ratio of areas from 1950 to 2019,

$$\mathrm{AF}_{\mathrm{UHI\ for\ 2019}} = \frac{\sum(\mathrm{UHI\ Area})_{2019}}{\sum(\mathrm{UHI\ Area})_{1950}} \tag{1}$$

Area estimates have been obtained in the next section in Table 3 between 1950 and 2019 time frames, yielding

Table 2 Global warming cause and effects

Global warming causes →	Population → Expanding Urban Heat Islands (UHI), Roads and Increases in Greenhouse Gas (GHG)
Global warming feedback amplification effects →	Water–Vapor Feedback, Land Albedo Change Due to Cities and Roads, Ice and Snow—Albedo Feedback, Lapse Rate Feedback, Cloud Feedback, etc.
Urban heat island solar amplification effects →	UHI Solar Heating Area (Building Areas), UHI Building Heat Capacities, Humidity Effects, Hydro-Hotspots, Reduced Wind Cooling, Solar Canyons, Loss of Wetlands, Increase in Impermeable Surfaces, Loss of Evapotranspiration Natural Cooling

the following results for the Schneider et al. [20] and the GRUMP [21] extrapolated area results:

$$AF_{\text{UHI for 2019}} = \frac{(\text{Urban Size})_{2019}}{(\text{Urban Size})_{1950}} \approx \begin{cases} \left(\dfrac{[0.188]_{2019}}{[0.059]_{1950}}\right)_{\text{Schneider}} = 3.19 \\ \left(\dfrac{[0.952]_{2019}}{[0.316]_{1950}}\right)_{\text{GRUMP}} = 3.0 \end{cases} \tag{2}$$

From the two studies, area scaling for the UHI solar amplification effect averages 3.1. Coincidently, this factor is the same observed in the Zhou et al. [31] study for the average footprint. This factor may seem high. However, it is likely conservative as other effects would be difficult to assess: increases in global drought due to loss of wetlands, deforestation effects due to urbanization, drought-related fires, and humidity issues. Also difficult to model are factor changes of other impermeable surfaces since 1950, such as city highways, parking lots, event centers, and so forth.

The 3.1 factor is one of the values used to weight the effective UHI area in the WAASU model between 1950 and 2019. It is applied as an UHI effective amplified solar (EAA_{UHI}) area giving more weight to the UHI albedo term. It is initially applied to the UHI area in Table 3 with an example given in Eq. 5. Appendix 1 and Eq. 4 describe the EAA_{UHI} concept.

2.2 Alternate method using the UHI's dome extent

An alternate approach to check the estimate of Eq. 3 is to look at the UHI's dome extent. Fan et al. [32] using an energy balance model to obtain the maximum horizontal extent of a UHI heat dome in numerous urban areas found the nighttime extent of 1.5 to 3.5 times the diameter of the city's urban area (2.5 average) and the daytime value of 2.0 to 3.3 (2.65 average). The horizontal extent of the heat dome is an important parameter for estimating the size of the area it influences and is similar to Zhou et al. [30] footprint.

In the Fan et al. method, the city diameter is multiplied by their derived day (2.65) and night (2.5) factors to obtain the horizontal extent. In our case, we want the diameter change from the area increase in Eq. 2, which is 1.8 $(=\sqrt{3.1})$. Therefore, this yields 2.5 × 1.8 = 4.5 higher in the night and 2.65 × 1.8 = 4.8 in the day in 2019 with an average of 4.65. According to Fan et al., this occurs 62.5% of the time. (Their study indicated that transition states are 4 h around sunrise, and about 5 h around sunset, and had less effect, totaling 9 h out of 24.) This yields an effective horizontal extent UHI amplification factor of 2.9. We note this is in good agreement with Zhou et al. footprint and Eq. 2. Fan et al. [32] assessed the heat flux over the urban area extends to its neighboring rural area where the air is transported from the urban heat dome flow. Therefore, the heat dome extends similarly as observed in the footprint studies. If we use the dome concept, we can assume that the actual surface area for the heat flux is increased as the surface area of the dome. This should be considered a measure of the atmospheric UHI vertical and horizontal extents which both are influential in global warming. We do not know the true diameter of the dome, but it is larger than the assessment by Fan et al. Using their dome extend applied to the area diameter D increase from 1950 to 2019, the amplification factor should be correlated to the ratios of the dome spherical surface areas:

$$AF_{\text{UHI for 2019}} = \left(\frac{D_{2019}}{D_{1950}}\right)^2 = 2.9^2 = 8.4 \tag{3}$$

This value is our second model assumption. Here the ratios of the dome's surface area are applied as an alternate approach in estimating how the amplification effect

Table 3 Extrapolated and amplified urbanized coverage estimates

Year	% Urban coverage of the Earth	Amplification factor	% Effective amplified area (EAA)
Schneider study [20]			
1950	0.059^a	1	0.059
2000-2001	0.51% × 0.29 = 0.148		
2019	0.188^a	3.1 AF^b_{Area}	0.459
2019	0.188^a	8.4 AF^b_{Dome}	1.143
Worst-case GRUMP study [21]			
1950	0.316^a	1	0.316
2000	2.7% × 0.29 = 0.783		
2019	0.952^a	3.1 AF^b_{UHI}	2.288
2019	0.952^a	8.4 AF^b_{Dome}	5.658

[a] Growth rate of cities using world population yearly growth rate in Fig. 1

[b] AF_{UHI} is the area amplification factor for 2019 referenced to 1950

scales with UHI growth which provides a measure of vertical and horizontal extent. Therefore, we use both, 3.1 and 8.4, as upper and lower bounds for the solar $\mathrm{EAA}_{\mathrm{UHI}}$.

2.3 Applying the amplification factors

In this analysis, 1950 is the reference year. Therefore, it is not subjected to amplification. Only the new UHI solar area is amplified as we are looking at changes since this time frame. The $\mathrm{EAA}_{\mathrm{UHI}}$ in 2019 (see Sect.2.5) can then be defined as

$$\begin{aligned}\mathrm{EAA}_{\mathrm{UHI}} &= \mathrm{AF}_{\mathrm{UHI}} \times \text{New area} + \mathrm{Area}_{1950} \\ &= \mathrm{AF}_{\mathrm{UHI}} \times \left(\mathrm{Area}_{2019} - \mathrm{Area}_{1950}\right) + \mathrm{Area}_{1950}\end{aligned} \tag{4}$$

Using this, if there were no changes in UHI solar growth, for example, so that the $\mathrm{Area}_{2019} = \mathrm{Area}_{1950}$, the resulting area is just the original Area_{1950} and if $\mathrm{AF}_{\mathrm{UHI}} = 1$, yields the 2019 unamplified area. This result is applied to the new area in Table 3.

2.4 Area extrapolations for 1950 and 2019

To assess the urbanized area, (also used in determining the UHI amplification factor ratios above), we need to project the Schneider [20] and GRUMP [21] area estimates down to 1950 and up to 2019. Both use datasets near 2000, so this is a convenient somewhat middle time frame. Here we decided to use the world population growth rate (World Bank [33]) which varies by year as discussed in Appendix 3 and shown in Fig. 1. We used the average growth rate per ½ decade for iterative projections of about 1.3% (from 2000 to 2019) to 1.8% (from 2000 down to 1955) per year.

To justify this projection, we see that Fig. 2a illustrates that building material aggregates (USGS [34]) as discussed in Appendix 3 used to build cities and roads correlate well to population growth (USGS Population Growth [35]).

It is also interesting to note that building materials for cities and roads also correlate well to global warming trends (NASA [36]) shown in Fig. 2b.

Column 2 in Table 3 shows the projections with the actual year (~2000) data point tabulated value also listed in the table (see also Table 1). The UHI area amplification factors (Column 3) are then applied to Schneider [20] and GRUMP [21] studies shown in Column 4 using Eq. 4.

As an example of the EAA calculation in Table 3, using Eq. 4, the 2019 Schneider 3.1 amplification factor is used as follows:

$$(0.188\% - 0.59\%) \times 3.1 + 0.59\% = 0.459\% \tag{5}$$

2.5 Weighted amplification albedo solar urbanization (WAASU) model overview

The WAASU model is very straightforward; the weighted model is rigorously derived in Appendix 1 and is based on a global weighted albedo model. The weighted solar albedo model for 1950 is

$$\alpha_{1950} = \frac{0.33}{A_{\mathrm{E}}} \sum \hat{A}_i \alpha_i + \frac{0.33}{A_{\mathrm{E}}} A_{\mathrm{UHI}}\, \alpha_{\mathrm{UHI}} + \frac{A_{\mathrm{C}}}{A_{\mathrm{E}}} \alpha_{\mathrm{C}} \tag{6}$$

, and for 2019 the WAASU model is

$$\alpha_{2019} = \frac{0.33}{A'_{\mathrm{E}}} \sum \hat{A}_i \alpha_i + \frac{0.33}{A'_{\mathrm{E}}} A_{\mathrm{UHI}} \mathrm{AF}_{\mathrm{UHI}}\, \alpha_{\mathrm{UHI}} + \frac{A_{\mathrm{C}}}{A'_{\mathrm{E}}} \alpha_{\mathrm{C}} \tag{7}$$

Here α is the Earth's Albedo, α_i is the albedo of each Earth component with the associated surface area $\hat{A}_i$ (the hat indicating all areas excluding the UHI area), similarly α_{UHI} is the UHI albedo associated with its area A_{UHI}, AF is the UHI amplification factor (Sects. 2.1 and 2.2), and A_{C} is the cloud coverage area with average cloud albedo α_{C} (Appendix 5). As explained in Appendix 1, the 0.33 factor arises from the fact that 67% of the Earth is approximately covered by clouds [37].

As well, A_{E} Earth's surface area in 1950 and A_{E}' is the Earth's area in 2019 due to the $\mathrm{EAA}_{\mathrm{UHI}}$ effective solar area increase, given by

$$A'_{\mathrm{E}} = \hat{A}_{\mathrm{E}} + \mathrm{EAA}_{\mathrm{UHI}} \tag{8}$$

Here EAA is defined in Eq. 4. Therefore, this increase requires renormalization that is discussed in Sect. 2.5.1. For example, if water covers 56% of the Earth, now it will be slightly less since the Earth's solar area has increased due to the buildup of cities since 1950 from the number of tall buildings that have increased the Earth's solar surface area along with other UHI amplification effects. This is captured in the solar effective amplified area.

It is important to note in the WAASU model (Eq. 7) that AF is combined with the UHI area and its albedo value

$$\left(A_{\mathrm{UHI}}\right)\left(\mathrm{AF}_{\mathrm{UHI}}\right)\left(\alpha_{\mathrm{UHI}}\right) \tag{9}$$

This shows the combined effect of the factor in the model and its possible influence on each factor. However, an assumption of the model is $\alpha_{\mathrm{UHI}} = 0.12$ and stays generally constant from 1950 to 2019. Average UHI albedo does not appear to vary much over time in the literature [38]. Therefore, consistent with Eq. 9 we find the amplification effect is mainly related to area growth as described in Sect. 2.1. This allows us to use the term as an effective amplified area (EAA) for the part $A_{\mathrm{UHI}} \times AF_{\mathrm{UHI}}$.

Note that all the effective surface areas are influenced by the solar irradiance

$$\text{Effective Surface Area} = \text{Surface Area} \times \%\text{Solar Irradiance}. \tag{10}$$

where the surface area includes all areas including EAA. However, we note that the change in the Earth Albedo over time (from 1950 to 2019) is just a function of the UHI area variation, (when holding all unrelated UHI components constant), that is

$$\left(\frac{d\alpha}{dt}\right)_{\mathrm{EA'}} \approx \sum \left(\text{Albedo}_{\mathrm{UHI}} \times \%\text{Solar Irradiance} \times \frac{d\,\text{Surface Area}_{\mathrm{UHI}}}{dt}\right)_i, \tag{11}$$

Here EA′ is all other Earth components (held constant). That is the main effect is the UHI surface area change from 1950 to 2019, the albedo and solar irradiance are considered constant.

2.5.1 Model constraints

Because of Eq. 8, this model is subject to the constraint

$$\text{Total Area} = \sum_i \{\%\,\text{Normalized Effective Amplified Surface Areas}_i\} + \%\text{Cloud Area} = 100\% \tag{12}$$

the small change in area $\mathrm{EAA}_{\mathrm{UHI}}$ will increase A_{E} slightly as described by Eq. 8. This requires renormalization to meet the requirements of Eq. 12. All areas change slightly including $\mathrm{EAA}_{\mathrm{UHI}}$. The UHI change is termed the normalization effective amplified area (NEAA). A full renormalization example is provided in Appendix 6.

To simplify things as much as possible, ***only five Earth constituents are used:*** *water, sea ice, land, UHI coverage, and clouds* (where *land* is its area minus the UHI coverage). These components are fairly easy to estimate, and references for their values are provided in Appendix 5. Furthermore, we use consistent values found in the IPCC AR5 report (Hartmann et al. [8]) assessment of the Earth's energy budget for solar irradiance. Table 4 summarizes the constraints from these IPCC values.

The fixed components of our model maintain relative consistency from 1950 to 2019. The non-fixed value is the urban coverage as indicated by Eq. 11. The only unknown value is the *land* albedo (minus the UHI coverage), and this value is adjusted to obtain the IPCC global albedo, 29.412%, and its Earth surface value of incident/reflected value of 7.059 (see Table 5a).

These values are used as a 1950 starting point, and then, the 2019 increase for the UHI coverage area is inserted. This increases the Earth's area to greater than 100%. Therefore, renormalization is done per the constraint of Eq. 12. Renormalization is detailed in Appendix 6.

3 Results

Using the extrapolated area coverage in Table 3 with the 3.1 amplification factor applied to the urbanized growth, the resulting global albedo change occurred of 29.399% in 2019 (Table 5b) compared to the earlier 1950 albedo value of 29.412% (Table 5a) for the Schneider nominal case. As well, for the GRUMP worst-case, the albedo changed from 29.412% (Table 6a) to 29.352% (Table 6b) due to the urbanized growth. Dome global albedo values are also provided in Appendix 6.

As we mentioned earlier, the increases in the solar surface area of the Earth, which will occur with city growth of tall buildings and their solar areas, however comparatively small, require renormalization of the Earth's surface components in the WAASU model (detailed in Appendix 6). This information is displayed in Column 3 in Tables 5b and 6b. While the model is sensitive to urban coverage changes, it works well with renormalization showing a high level of consistency to urban coverage proportionality changes. This consistency is indicated in Table 7 where we find the GRUMP and Schneider long wavelength radiation (LWR) forcing per %EAA averages about 0.096% (W/m^2)/%NEAA in the last column.

Table 7 provides a summary of albedo changes found in the WASSU model along with the expected solar longwave radiation increase. From the above global WAASU model, the estimates of the Earth's LWR emissions are obtained from the fundamental expression

$$P_\alpha = \mathbf{340}\ \mathrm{W/m^2}(1 - \text{Albedo}). \tag{13}$$

Then, the albedo change from 1950 to 2019 represents the equivalent increase in LWR is given by

$$\Delta P_\alpha = \mathbf{340}\ \mathrm{W/m^2}\left\{(1 - \text{Albedo})_{2019} - (1 - \text{Albedo})_{1950}\right\}. \tag{14}$$

The results are compiled in Table 7. The table also includes "What if" estimates, if we could change urbanization to be more reflective with cool roofs to reverse the effect.

The overall results are summarized:

- Schneider nominal case from 1950 to 2019, the increase in LWR forcing (Row 7) is 0.042 W/m^2 and 0.11 W/m^2 due to urban area and dome amplification coverage, respectively. These values do not include the addition of GHG re-radiation (see Table 8).

- GRUMP worst-case from 1950 to 2019 the increase in LWR (Row 7) is 0.204 W/m^2 and 0.537 W/m^2 due to urban area and dome amplification coverage, respectively. These values do not include the addition of GHG re-radiation (see Table 8).

Table 4 IPCC Earth energy budget values (Hartmann et al. [8])

IPCC item 2013 budget	Incident and reflected radiation (W/m^2)	Albedo % α	P_α^a Absorbed (W/m^2)
Earth	100/340	29.412	240 = 340 × (1–0.294)
Atmosphere and clouds	76/340	22.353	79
Earth surface albedo	24/340	7.059	161
Year	GHG effect^a	Surface T (°K)^a	Power
1950 No GHG effect	$P_\alpha \times 1$	255 (– 18.09 °C)	240
1950 With GHG effect	$P_\alpha \times 1.62^a$	287.3 (14.6 °C)	388.8 (= 240 × 1.62)

[a] $1.62 \approx \beta^4$, effective emissivity of the planetary system (average GHG re-radiation factor), $P_\alpha = 340$ W/m^2 $(1-\alpha)$, and $T = (P/\sigma)^{0.25}$

Table 5 (a) Schneider 1950 effective estimate. (b) Schneider 2019 effective estimate (AF = 3.1)

(a)

Surface	Albedo	%NEAA	Cloud effect %NEAA	Weighted albedo %
	A	B	$C = B \times (1–0.67)$	$A \times C$
Sum of water type		71		
Sea ice	0.6	15	4.95	2.970
Water	0.06	56	18.48	1.109
Sum of land type		29		
Land – (UHI + Coverage)	0.312	28.941	9.551	2.978
UHI + Coverage	0.12	0.059	0.02	0.002
		∑ = 100.000	33.000	7.059
			Cloud area	
Clouds	0.334	67	67	22.353
∑ Sum Earth %			100.000	
∑ Global Albedo				29.412

(b)

Surface	Albedo	%NEAA	Cloud effect %NEAA	Weighted albedo %
	A	B	$C = B \times (1–0.67)$	$A \times C$
Sum of water type		70.717		
Sea ice	0.6	14.94	4.930	2.958
Water	0.06	55.777	18.406	1.104
Sum of land type		29.283		
Land – (UHI + Coverage)	0.312	28.826	9.513	2.966
UHI + Coverage	0.12	0.4571	0.151	0.018
		∑ = 100.000	33.00	7.028
			Cloud area	
Clouds	0.334	67	67	22.353
∑ Sum Earth %			100.000	
∑ Global Albedo				29.399

- The forcing per unit %NEAA or %EAA has consistency with small variability and averaging about 0.096 *W/m^2/%NEAA*. We also note in Column 8 the consistent value of 1.0 W/m^2/%Δalbedo. This is the percent change from the initial albedo value of 29.413%. This value is a useful constant and can be derived [39]. Note these values do not include GHG re-radiation (see Sect. 4).
- "What if" corrective action results of cool roofs indicate that changing city albedos in both the Schneider and the GRUMP case from 0.12 to an average value of 0.205 would reverse the increase forcing back to 1950 levels. By comparison, He et al. [40] found the average albedo varies from 0.1 to 0.4, averaging 0.25. Note our model found the average land albedo slightly higher at 0.31 (Tables 5 and 6).

4 Discussion on the relative contribution to global warming forcing due to UHIs

In this section, the LWR results in Table 7 are adjusted by including GHG re-radiation forcing that will additionally occur. As well, the total global warming forcing contributions are described.

4.1 Full UHI radiation forcing and associated temperature rise

Estimates in Table 7 provide the LWR forcing, but the anticipated average GHG additional re-radiation forcing increase expected is not included. This average re-radiation GHG factor is roughly estimated as 1.62 [39] (this 62% factor is approximately equal to β^4, the effective emissivity of the planetary system) and is exemplified in Table 4. Table 8, Column 4 provides the forcing when the 1.62

Table 6 (a) GRUMP 1950 effective estimate. (b) Grump 2019 effective estimate (AF = 3.1)

(a)

Surface	Albedo *A*	%NEAA *B*	Cloud effect %NEAA *C* = *B* x (1–0.67)	Weighted albedo % *A* x *C*
Sum of water type		71		
Sea ice	0.6	15	4.95	2.970
Water	0.06	56	18.48	1.109
Sum of land type		29		
Land – (UHI + Coverage)	0.314	28.684	9.466	2.968
UHI + Coverage	0.12	0.316	0.104	0.013
		∑ = 100.000	33.000	7.059
			Cloud area	
Clouds	0.334	67	67	22.353
∑ Sum Earth %			100.000	
∑ Global Albedo				29.412

(b)

Surface	Albedo *A*	%NEAA *B*	Cloud effect %NEAA *C* = *B* x (1–0.67)	Weighted albedo % *A* x *C*
Sum of water type		69.627		
Sea ice	0.6	14.71	4.854	2.913
Water	0.06	54.917	18.123	1.087
Sum of land type		30.373		
Land – (UHI + Coverage)	0.314	28.129	9.283	2.910
UHI + Coverage	0.12	2.244	0.740	0.089
		∑ = 100.000	33.000	6.910
			Cloud area	
Clouds	0.334	67	67	22.353
∑ Sum Earth %			100.000	
∑ Global Albedo				29.352

Table 7 Albedo and radiative increase model results with UHI effective area

Year	UHI area %	UHI %EAA AF = 3.1 AF = 8.4	UHI NEAA Global surface %area	Albedo cities	Global weighted albedo %	Forcing LWR[a] ΔP_α UHI W/m^2	$\frac{\Delta P_\alpha\,(W/m^2)}{\%NEAA}\left(\frac{\Delta P_\alpha\,(W/m^2)}{\%Albedo}\right)$
Nominal case Schneider study (2019 dome and footprint)							
1950	0.059	0.059	0.059	0.12	29.412	0	–
2019	0.188	0.459	0.457	0.12	29.399	0.044	0.096 (1.0)
2019	0.188	1.143	1.131	0.12	29.379	0.112	0.10 (1.0)
What if	0.188 0.188	0.459 1.143	0.457 1.13	0.202 0.209	29.412	−0.042 −0.113	–
Worst-case GRUMP study (2019 dome and footprint)							
1950	0.316	0.316	0.316	0.12	29.412	0	–
2019	0.952	2.288	2.243	0.12	29.352	0.204	0.091 (1.0)
2019	0.952	5.658	5.395	0.12	29.255	0.534	0.099 (1.0)
What if	0.952 0.952	2.288 5.658	2.244 5.395	0.201 0.209	29.412	−0.204 −0.537	–

[a] LWR Forcing values do not include the additional GHG re-radiation (see Table 8)

factor GHG re-radiation is included and Column 5 shows the associated temperature increase. Appendix 7 provides an overview with a detailed estimate of the forcing and temperature rise assessments found in Table 8.

4.2 IPCC/NOAA radiation forcing comparison

To make relative comparisons with UHI forcing, we compare the forcing results in Table 8 to the IPCC estimate for GHG forcing from the period 1950 to 2019, and GHG warming associated temperature rise. The GHG forcing estimate by IPCC/NOAA [41] is 2.38 W/m^2 during this period.

One should note that this value does not include "feedback" (i.e., arctic snow and ice melting) discussed in our conclusions. Column 6 in Table 8 shows the relative forcing ratio to compare it to the UHI strength. For example, the LWR found in the Schneider case for the albedo of 29.3994 was 0.044 W/m^2 in Table 7. Then, we estimate with GHG re-radiation as 0.044 W/m^2 × 1.62 = 0.071 W/m^2 in Column 4 and relative to the IPCC GHG forcing estimate is about 3% (= 0.071/2.38) in Column 6, Table 8. One can also obtain the same percentages in Column 6 by dividing the temperature increase in Column 5 by 0.44 °C. Here 0.44 °C is the temperature rise one obtains from IPCC/NOAA 2.38 W/m^2 of forcing without feedback (see Appendix 7) which is a little less than half of the total warming observed since 1950. Note that only Column 6 uses IPCC/NOAA estimates in our results. In the conclusion, we discuss another method using a feedback approach that increases these estimates somewhat as shown in the last column.

Finally, the forcing estimate in Column 8, Table 7 is updated in Table 8 from Column 4 divided by Column 3 as

$$\begin{aligned}\alpha_{\text{Global\_Forcing}} &= 1.62 \times 1.0\ \text{W/m}^2/\%\Delta\text{Albedo}\\ &= 1.62\ \text{W/m}^2/\%\Delta\text{Albedo}\end{aligned} \tag{15}$$

and from Table 8, Column 4 divided by Column 1, the consistent forcing per %EAA estimate is

$$\text{UHI}_{\text{EAA\_Forcing}} \approx 1.62 \times 0.096\ \text{W/m}^2/\%\text{EAA} = 0.16\ \text{W/m}^2/\%\text{EAA} \tag{16}$$

where the %EAA is given by Eq. 4 and exemplified in Eq. 5. Examples of how these might be used are provided

Table 8 WAASU Model full forcing and global warming estimate due to UHI in 2019

UHI EAA global surface %Area	Global weighted albedo	Percent albedo change from 29.412	Full UHI forcing P_α includes GHG re-radiation LWR × 1.62 W/m^2	UHI Temperature ΔT_{UHI} (°C)	UHI GW percent relative to IPCC/NOAA GHG forcing of 2.38 W/m^2	UHI GW percent based on feedback method
Schneider case						
0.459	29.399	0.044%	0.071 (Footprint)	0.013	3	3.3
1.143	29.379	0.11%	0.182 (Dome)	0.034	7.6	8.5
GRUMP case						
2.288	29.352	0.2%	0.33 (Footprint)	0.061	13.8	15.3
5.658	29.255	0.53	0.865 (Dome)	0.16	36.3	40

in Appendix 7. Lastly, as a check, one may note that UHI global warming estimates roughly scales with UHI size as might be expected. For example, in Table 1 the ratio of Schneider to Grump UHI area extent is 2.7/0.51 = 5.3. We note the values in the last column in Table 8 scale close to this factor (i.e., 3% × 5.3 = 15.9% which is close to 13.8% and 7.6% × 5.3 = 40% close to 36%) between Schneider and GRUMP, respectively. Inexact scaling is due to Eq. 4.

5 Conclusions

In this paper, we derived a versatile WAASU model and applied it to provide estimates of the UHI effect (with urban areas) on global warming. This calculation was done with the aid of assumptions for UHI solar amplification factors. These estimates inserted into our WAASU model found that between 0.071 and 0.87 W/m^2 of radiative forcing (Table 8) may be possible. This forcing result indicates that about 3% to 36% of global warming may be due to the UHI effect by comparisons to anticipated IPCC/NOAA GHG forcing values with median and mean GW relative percentages of 10.7% to 15.2%, respectively. In this conclusion, we provide an alternate method that includes feedback and which finds slightly larger but comparable warming estimates due to UHIs. This method includes ice loss results in Appendix 4, which found warming feedback using a related WAS model yielded a 0.15 °C rise. This ice loss feedback represents about 16% of GW in 2019 relative to the 0.95 °C estimated increase since 1950.

The wide variations we found on forcing values are due to both the amplification and urban area uncertainties which we now provide guidance for in this conclusion. However, the model found that the forcing per effective amplified UHI area and albedo estimates were consistent showing 0.16 W/m^2/%EAA and 1.62 W/m^2/%Δalbedo, respectively (see Eqs. 15 and 16). Note that if better estimates are known for the %EAA, (see Eq. 4), then one can quickly assess the impact of the UHI GW effect using the 0.16 W/m^2/%EAA estimate.

The WAASU model is versatile. We can quickly look at UHI albedo changes required to offset the estimated forcing. For example, "What if" corrective action results of cool roofs indicated that an average UHI albedos change from 0.12 to 0.21 would reverse the UHI forcing back to 1950 levels. This value was found to be close to the average global land surface albedo of 0.25 [40]. This suggests that the cooling potential of UHIs is very high. For example, if cool roofs and other worldwide changes can be made to raise the UHI albedo to 0.48, (fourfold higher in reflectivity), then this reverse forcing could likely reduce global warming by about 30% or more (estimated from median albedo values).

Therefore, the model can provide albedo-area estimates for reverse forcing similar to the "What if" corrective actions for mitigation/adaptation strategies. As a follow-up study, the author has proposed a similar modeling strategy to estimate select areas changes necessary for surface albedo type global warming solutions [39].

To provide an alternate estimate of the influence that UHIs play in global warming, consider the following temperature breakdown:

$$\Delta T = T_{\mathrm{GHG}} + T_{\mathrm{U\text{-}A}} + T_i + T(\lambda_{\mathrm{WV}}, \lambda_{\mathrm{I}}) + T(\lambda_{\mathrm{A}}, \lambda_{\mathrm{LR}}, \lambda_{\mathrm{C}}, \lambda_{\mathrm{U}}) \text{ and } T_{\mathrm{U\text{-}A}} = T_{\mathrm{UHI}} + T_{\mathrm{O\text{-}U}} \tag{17}$$

Here $\Delta T = 0.95$ °C is the temperature rise from 1950 to 2019, with contributions from GHG (T_{GHG}), urbanization-albedo land-use/land-cover issues (**$\mathbf{T}_{\mathbf{U}\text{-A}}$**), UHIs ($T_{\mathrm{UHI}}$), other urbanization-albedo land-use/land-cover effects (rural roads, rooftops, etc.) ($T_{\mathrm{O\text{-}U}}$), and other possible smaller temperature rise effects (aerosols, soot on snow, etc.) (T_i). These are all temperature rises related to direct forcing.

$T(\lambda)$ represents warming due to feedbacks. They are a function of feedbacks responses (water vapor (WV), (I) ice loss, other albedo (A) issues, lapse rate (LR), clouds (C), and (U) urbanization related feedback).

In an article by Liu et al. [42], urbanization area is categorized in an attempt to clarify uncertainties due to the various definitions of what is urban and the wide assessments among authors on how much of the Earth has been urbanized. According to Liu et al., the GRUMP area estimate fits the definition of "urban area," where the Schneider estimate fits the definition of "built-up area". Therefore, considering their recommendation, we favor the dome amplification estimate for Schneider as it provides a measure of horizontal and vertical warming area extent from land-use/land-cover albedo UHI effects. Although $T_{\mathrm{A\text{-}U}}$ is dominated by T_{UHI}, the GRUMP footprint provides a horizontal extent that can be used as a weighting factor in estimation to account for $T_{\mathrm{O\_U}}$ as it incorporates a larger area. Therefore, this leads to our recommendation for using the median value in Table 8 in Eq. 17 for $T_{\mathrm{U\text{-}A}}$.

Note that the median $T_{\mathrm{U\text{-}A}}$ value is weighted 30% (0.0475 °C/0.16 °C) GRUMP and 70% Schneider (where 0.16 °C is the upper GRUMP estimate in Table 8). Then from rows 4 and 5 in Table 8, we recommended the following:

$$T_{\mathrm{U\text{-}A}} = \{0.0475\,^{\circ}\mathrm{C}\ (\text{Median value}) \text{ and } F_{\mathrm{U\text{-}A}} = \{0.256\ \mathrm{W/m^2}\ (\text{Median value}) \tag{18}$$

Then let

$$T(\lambda_{\mathrm{I}}, \lambda_{\mathrm{WV}}) \approx 0.15\,^{\circ}\mathrm{C} + \left[(T_{\mathrm{GHG}} + T_{\mathrm{U\text{-}A}})\right]_{\mathrm{WV}} \text{ and } T_i + T(\lambda_{\mathrm{A}}, \lambda_{\mathrm{LR}}, \lambda_{\mathrm{C}}, \lambda_{\mathrm{U}}) \geq 0 \tag{19}$$

The inclusion of the $\mathbf{T_{A\text{-}U}}$ term provides a measurable way to take into account this work. This result can be compared to other authors who have contributed to the understanding of global warming influences from UHIs [1–3, 6, 7, 9–17]. Equation 19 is based on the results of Appendix 4 for ice loss (0.15 °C). The water vapor feedback factor in Eq. 19 of one-time forcing estimates is based on the findings of other authors [27–29].

The feedback term, $\boldsymbol{\lambda_U}$, is difficult to quantify with high confidence, but it is important to account for UHI effects. Here, we point out several key UHI feedbacks effects that have been studied and play a role in global climate change (see also Appendix 2):

1. In a study of wetland reduction in China and its correlation to drought, Cao et al. [43] looked at the wetland distributions and areas for five provinces due to urbanization. These areas showed a total reduction in southwestern China from 1970 to 2008 of 17% ground area, with the highest reduction rate occurring from 2000 to 2008. They found these changes to the wetland area showed a negative correlation with temperature (i.e., wetland decrease, increase in temperature), and a positive correlation with precipitation (i.e., wetland decrease, precipitation decrease). One can conclude that albedo management of urbanization would help increase the loss in condensation. Although some cities find increases in precipitation due to complex warming turbulence, the larger picture indicates that UHIs are a cause of drought. Of course, drought is also the result of other global warming forcing issues in Eq. 17.
2. Drought feedback leads to forest fire feedbacks that not only damage forests that would otherwise remove CO_2 from the air, but that also releases CO_2 and other GHGs into the atmosphere. Therefore, this is a major offset in CO_2 worldwide reduction efforts. This suggests the urgent need for supplementary albedo reverse forcing efforts. Albedo reverse forcing efforts can also be offset by a lack of albedo controls in urbanization development. Therefore, if progress is to be made in climate change mitigation, it is imperative to work on both CO_2 and albedo UHI management.
3. Zhao et al. [44] observed that UHI temperatures increase in daytime ΔT by 3.0 °C in humid climates but decrease ΔT by 1.5 °C in dry climates. They found a strong correlation between ΔT increase and daytime precipitation. Their results concluded that albedo management would be a viable means of reducing ΔT on large scales.
4. This effect is often attributed to greenspace decrease of surface roughness due to UHI impermeable smooth surfaces which reduces convection cooling efficiency (Zhao et al. [44], Gunawardena et al. [45])
5. In general, UHIs lessens the possibilities for the evapotranspiration process and thereby reduces the natural cooling effect since vegetation is scarce. UHI cause higher rates of movement of water from the soil, plants, and pavement precipitation evaporation into the atmosphere. Since hotter air can hold more water, it exacerbates dryness. This can promote a local GHG effect and be partly responsible for the observed warming. These effects may to a lesser extend occur on all smooth hot evaporating surfaces (during precipitation periods) including roads and highways.
6. Another problem is due to the large heat capacity of cities that increase the length of warming time after sunset. Nighttime warming creates longer dry periods and also contributes to drought conditions and the potential for forest fires.
7. Lastly, any additional global warming due to $\mathbf{T_{A\text{-}U}}$ can contribute to other positive feedbacks in Eq. 17 as indicated by Eq. 19.
8. The primary mitigating factor in all these cases would be albedo UHI management of impermeable surfaces.

We now refine our GW UHI estimate by including a feedback method with Eq. 19. We first consider the quantity $T_i + T(\lambda_A, \lambda_{LR}, \lambda_C, \lambda_U)$ to be small (as we do not have knowledgeable estimates) and approximated it as zero to simplify. Then solving Eqs. 17–19, with $\Delta T = 0.95$ °C, the following results are obtained

$$T_{\text{U - A}} + T_{\text{GHG}} = 0.0475\,^{\circ}\text{C} + 0.3525\,^{\circ}C = 0.4\,^{\circ}\text{C (Median value)} \tag{20}$$

This gives the following global warming root cause estimates due to urbanization for $T_{U\text{-}A}$ as

$$\text{GW}\%(T_{\text{U - A}}) = 0.0475\,^{\circ}\text{C}/\,0.4\,^{\circ}\text{C} = 11.9\%\ \text{(Median value)} \tag{21}$$

Other values are provided in Table 8, Col. 7. We have now provided two different types of assessments; the IPCC/NOAA and feedback methods that have yielded similar median assessments of 10.7% and 11.9%, respectively. These two estimates are in reasonable agreement and provide an average of 11.3%. This agreement also suggests that our ice loss temperature feedback increase estimate of 0.15 °C in Appendix 4 (using the WAS model) is reasonable. Equation 21 suggests that a little forcing (0.4 °C) can create a lot of feedback and is a primary problem in global warming. In the introduction, it was noted that Zhao and Huang et al. [14, 16] found that about 30% of GW could be due to UHIs. Therefore, our median estimate is a little more than one-third in comparison providing some support. (Full support would require upper bound estimates in Table 8.) It should also be noted in the WAASU model, we were very conservative with cloud coverage, allowing only 33% of solar radiation to reach the Earth through clouds (see Appendix 1), as some attenuated sunlight normally radiates through. The results actually ratios with cloud coverage. For example, if the cloud/atmosphere coverage used was less conservative and closer to an IPCC estimate of 47% (Table 4, 161/340=0.47), then the increase in global warming due mainly by UHIs would go from 11% to about 16% (16%=0.47/0.33x11%).On the other hand, feedbacks are difficult to quantify, and we noted in Appendix 4 that our temperature rise due to ice loss is a rough estimate due to numerous uncertainties encountered by climatologists in fully quantifying the seasonal variations in ice changes. Furthermore, water vapor feedback estimates may be lower than the factor of one-time forcing suggested by some authors [27–29].

We conclude that about 11%–16% of global warming is due primarily to the UHI effect based on our median estimates in Table 8. This estimate would likely increase if other feedbacks were included. However, this provides strong engineering judgment that land-use/land-cover albedo effects (i.e., UHI and land-use changes) are responsible for an important portion of global warming and that albedo management of urbanization is an urgent matter. Left unattended along with urbanization expected growth, the influence of UHIs will continue to offset CO_2 reduction efforts and increasingly contribute to warming and feedback issues. Furthermore, proper worldwide albedo urbanization management would lead to a substantial reversal of global warming trends [39].

Below, we provide suggestions and corrective actions, which include:

- Modification of the Paris Climate Agreement to include albedo controls and solutions
- Albedo guidelines for UHI impermeable surfaces, cool roofs, and roads similar to ongoing CO_2 efforts
- UHI albedo goals: we suggest an albedo increase by a factor of 4 (from 0.12 to 0.48), which could reduce GW by about 30% or more, assessed from our median ranges and other studies [39, 46, 47].
- Government funding for geoengineering and implementation of albedo solutions
- Centralize albedo solution efforts in a single government agency (possibly NASA)
- Guidelines for future albedo design considerations of urbanization areas
- Further development of white solar cells and their use for cooler panels
- Requires cars to be more reflective. Although worldwide vehicles do not comprise much of the Earth's solar area, recommending the preferential manufacturing of cars that are higher in reflectivity (e.g., silver or white) would raise awareness of this issue similar to electric automobiles that help improve CO_2 emissions.

Acknowledgements The author would like to thank the reviewers for their valuable comments on the paper.

Compliance with ethical standards

Conflict of interest The author declares that he has no conflicts of interest.

Appendix 1: Derivation of the WASSU and WAS models

The Earth's long wavelength radiation power P in W/m^2 is given by

$$P = \frac{S_o}{4}(1 - \alpha) \tag{22}$$

Here α is the Earth's albedo and S_o= 1360 W/m^2. From Eq. 22, the albedo can be written

$$\alpha = 1 - \frac{4P}{S_o} \tag{23}$$

Let small p indicate the power in watts so that

$$p(\text{watts}) = A_E\ P(\text{W/m}^2) \tag{24}$$

This is useful for rewriting Eq. 22 in terms of the Earth's areas A_E for surface land area A_S and cloud coverage area A_C, receiving solar power. This gives

$$p(\text{watts}) = A_E\frac{S_o}{4}(1-\alpha) = (A_S + A_C)\frac{S_o}{4}(1-\alpha) = (0.33A_E + A_C)\frac{S_o}{4}(1-\alpha) \tag{25}$$

Here it is assumed that on average 33% of the Earth receives direct sunlight or 67% is covered by clouds [Ref. [37], Appendix 5], that is the Earth's primary solar area is

$$A_E = A_S + A_C = 0.33A_E + A_C \tag{26}$$

Now we can divide Eq. 25 through by A_E and the $S_o/4$ term and expand out the Earth's areas as

$$\frac{4p}{A_E S_o} = \frac{4P}{S_o} = \frac{(0.33A_E + A_C)}{A_E}(1-\alpha) = \frac{0.33}{A_E}\sum A_i(1-\alpha_i) + \frac{A_C}{A_E}(1-\alpha_C) \tag{27}$$

Here A_i and A_c are surface area and cloud area coverages, while α_i and α_c are their associated albedo values. Then expanding terms on the RHS, we have

$$\frac{4P}{S_o} = \frac{0.33}{A_E}\sum A_i - \frac{0.33}{A_E}\sum A_i\alpha_i + \frac{A_C}{A_E} - \frac{A_C}{A_E}\alpha_C \tag{28}$$

Collecting terms we can write

$$\frac{4P}{S_o} = \left\{\frac{0.33}{A_E}\sum A_i + \frac{A_C}{A_E}\right\} - \frac{0.33}{A_E}\sum A_i\,\alpha_i - \frac{A_C}{A_E}\alpha_C \tag{29}$$

Note that in Eq. 29 the first term on the RHS is unity

$$\left\{\frac{0.33}{A_E}\sum A_i + \frac{A_C}{A_E}\right\} = \frac{A_S + A_C}{A_E} = 1 \tag{30}$$

Then, Eq. 29 is now

$$\frac{4P}{S_o} = 1 - \left(\frac{0.33}{A_E}\sum A_i\alpha_i + \frac{A_C}{A_E}\alpha_C\right) \tag{31}$$

or

$$1 - \frac{4P}{S_o} = \frac{0.33}{A_E}\sum A_i\,\alpha_i + \frac{A_C}{A_E}\alpha_C \tag{32}$$

Combining this with Eq. 23, the weighted albedo solar (WAS) model is

$$\alpha = \frac{0.33}{A_E}\sum A_i\,\alpha_i + \frac{A_C}{A_E}\alpha_C \tag{33}$$

However, further weighting the model with the UHI amplification factor AF_{UHI} by expanding out A_i to treat the UHI area separately yields our final Weighted Amplification Solar Urbanization (WAASU) model

$$\alpha = \frac{0.33}{A_E}\sum \hat{A}_i\alpha_i + \frac{0.33}{A_E}A_{UHI}AF_{UHI}\,\alpha_{UHI} + \frac{A_C}{A_E}\alpha_C \tag{34}$$

The inclusion of AF_{UHI} is presented as a weighting factor in the only logical part of the equation for the WAASU model. Here, the first term $\hat{A}_i$ with the hat indicates all surface areas of the Earth except the UHI area, and the second term is broken out for the UHI sum to include the AF term. We note that $AF_{\mathbf{UHI\_1950}}=1$ and $AF_{\mathbf{UHI\_2019}}>1$ (see Sects. 2.1 and 2.2 for this factor). Note that we take $\alpha_{UHI}=0.12$ [48] as constant from 1950 to 2019, then $A_{UHI}\times AF_{UHI}$ can be considered as an effective area amplification factor. The $\alpha_{UHI}=0.12$ [48] appears somewhat on the low end for average UHI albedos from some studies [38]. However, in general, albedo reporting appears somewhat constant in time over city growth [38].

Appendix 2: UHI dominant amplification effects and climate effects

The UHI amplification effects that we consider to dominate listed in Table 2 are as follows:

- *The heat capacity and solar heating area amplification effect:* Solar surface areas of buildings make the city much larger than its actual surface area in terms of solar absorption. Thus, solar building area amplification may be the most dominant aspect of the UHI climate area. When this is included with the massive heat capacities of building, the combined effect creates a day-night heat cycle. In most cities, it is observed that daytime atmospheric temperatures are cooler compared to night. For example, in a study by Basara et al. [49] in Oklahoma city UHI, it was found that at just 9-m height, the UHI was consistently 0.5–1.75 °C greater in the urban core than the surrounding rural locations at night. Further, in general, the UHI impact was strongest during the overnight hours and weakest during the day. This inversion effect can be the result of massive UHI buildings acting like heat sinks, having giant heat capacities, and storing heat in their reservoir via convection as solar radiation is absorbed during the day. This occurrence often reduces the UHI day effect, but at night buildings cool down, giving off their stored heat that increases local temperatures to the surrounding atmosphere. This effect increases with city growth as buildings have gotten substantially taller since 1950 (Barr [50]).

- *The hydro-hotspot amplification effect:* This effect is not well addressed in the literature. Atmospheric moisture source is a complex issue due to hydro-hotspots (HHS). HHS occurs when buildings are hot due to sun exposure. Then, during precipitation periods, the hot evaporation surfaces increase localized water vapor as warm air holds more moisture. This increase likely acts at times as a local greenhouse gas that blankets city heat and increases infrared radiation during these periods, providing another UHI humidity amplification source. This effect combined with the heat storage occurring from daytime hours indicates that the effect may occur even during nighttime precipitation. The level of hydro-hotspot significance in climate change is currently unknown. However, observations of this effect are reasonably well established in observed humidity effects.
- *The humidity amplification effect:* This effect has been observed. For example, Zhao et al. [44] noted that UHI temperature increases in daytime ΔT by 3.0 °C in humid climates but decreasing ΔT by 1.5 °C in dry climates. They noted that such relationships imply UHIs will exacerbate heat wave stress on human health in wet UHI climates. They found a strong correlation between ΔT increase and daytime precipitation. Their results concluded that albedo management would be a viable means of reducing ΔT on large scales.
- *Reduced wind cooling and solar canyons:* In UHIs reduced wind is a known effect due to building wind friction that inhibits cooling by convection. Tall buildings also create solar canyons and trap sunlight, reducing the average albedo, although some benefits occur from shading. In general, both have the effect of amplifying the temperature profile of UHIs.

Many of these amplification effects create local and global climate issues for over 50% of the world population that now lives in cities. We summarize theses climate issues as follows:

- UHIs are warmer than their rural vicinities and create a dome of warmer air above cities.
- Wind reduction due to building resistance create cooling losses.
- Often city rainfall rates are noticeably higher. Common hypotheses include the fact that warm air creates turbulence and pollution supplies extra nuclei that encourage cloud rain droplets.
- Increases in the evaporation rate from hot impermeable surfaces during precipitation (hydro-hotspots) can increase atmospheric GHG water vapor contributing to a local temperature increase (see next bullet).
- UHI temperatures increase in daytime ΔT by 3.0 °C in humid climates but decrease ΔT by 1.5 °C in dry climates [44]. A strong correlation has been found between ΔT increase and daytime precipitation. Their results concluded that albedo management would be a viable means of reducing ΔT on large scales.
- This humidity effect may extend the daytime issue into nighttime depending on a city's heat capacity.
- Because of the increase in air pollutants, including CO_2 from automobiles, there is an increase in the GHG warming effect as compared to non-urban areas.
- Reduction of natural vegetation in UHIs lessens the possibilities for the evapotranspiration process and thereby reduces the natural cooling effect since vegetation is scarce.
- The UHI dome/footprint increases evapotranspiration losses into the nearby rural areas and the cities heat capacity increases the length of time these losses occur.
- Impervious surfaces add to the loss of evapotranspiration with increases water runoff compared to rural areas.
- Increases in the evaporation rate also create warmer ground temperatures over longer periods creating dryness and including local forest that can be prone to fires.
- Anthropogenic heating creates some surface temperatures increases, also amplifying the UHI effect.
- The accumulation of these effects increases the man-made UHI thermal forcing mechanism that adds to global warming and potentially can escalate the feedback climate inertia warming problems as well.

Appendix 3: Growth rates and information on natural aggregates

Figure 1 is a plot of the world population growth rate that varies from about 2.1% to 1.1%. This graph is used to make growth rate estimates of urban coverage. We note that natural aggregates used to build cities and roads are reasonably correlated to population growth in Fig. 2a. Also of interest (Fig. 2b) is the fact that one can see some correlation to global warming with the use of natural aggregates.

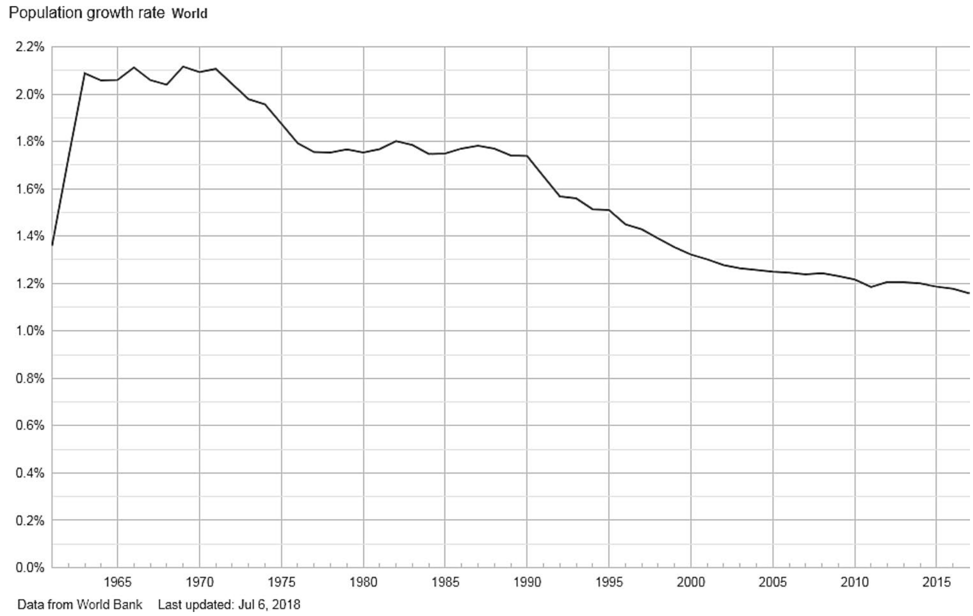

Data from World Bank Last updated: Jul 6, 2018

Fig. 1 Population growth rate by year from 1960 to 2018, World Bank, [33]

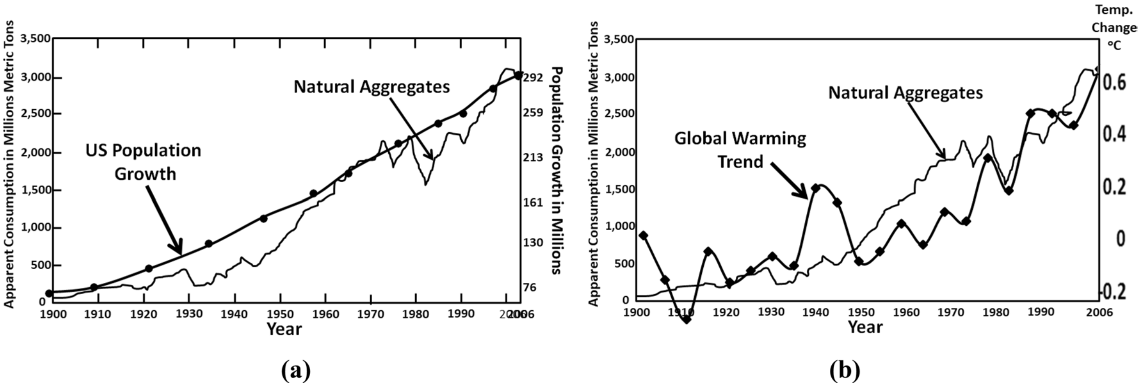

Fig. 2 **a** Natural aggregates [34] correlated to US Population Growth (USGS [33]) **b** Natural aggregates [33] correlated to global warming (NASA [36])

Appendix 4: Weighted albedo solar model applied to the melting of sea ice

The weighted albedo solar (WAS) model (Eq. 33) derived in Appendix 1 can be used to estimate the warming feedback due to sea ice loss in the Arctic. We need to make several initial estimates to obtain a ballpark number of warming due to sea ice loss. The first estimate is that the Antarctic sea ice has remained roughly constant (NOAA, Scott [51]) over the last two decades. Next, it is estimated that the Arctic sea ice area is about 60% larger on average compared with Antarctic sea ice areas yearly (NOAA, Scott [51]). It has been observed that the Arctic sea ice is melting at an alarming rate of 12.85% per decade in the last two decades (NASA sea ice [52]). This apparent trend appears to yield an estimated 25.7% decrease in sea ice in the last two decades. It is difficult to find a strong reference for quantifying global warming impact due to Arctic sea ice melting. However, we can get an approximation from the WAS model (and further illustrate the strengths of these models). Sea ice melting will result in a significant albedo change that roughly changes the ice-albedo of 0.6, to the open ocean albedo of 0.06 (see Tables 9 and 10). Fortunately, the Arctic areas receive only about 40% as much solar radiation (Sciencing [53]) reducing the feedback effect. From Eq. 10, the effective sea ice surface area reduction from the irradiance decrease can be approximated as

$$\text{Effective Arctic Sea Ice Surface Area} = 0.6 \times 15\%\{1 - (0.257 \times 0.40)\} = 8.064\% \tag{35}$$

Table 9 Baseline (Albedo = 29.412, 1950)

Surface	Albedo	%Area	Cloud effect %NEAA	Weighted Albedo %
	A	*B*	*C* = *B* × (1–0.67)	*A* × *C*
Sum of water type		71		
Sea ice	0.6	15	4.95	2.970
Water	0.06	56	18.48	1.109
155 sum of land type		29		
Land – (UHI + Coverage)	0.312	28.941	9.551	2.978
UHI + Coverage	0.12	0.059	0.02	0.002
		∑ = 100.000	33.000	7.059
			Cloud area	
Clouds	0.334	67	67	22.353
∑ Sum Earth %			100.000	
∑ Global Albedo				29.412

Table 10 Sea ice loss—albedo change (29.2443%, 2019)

Surface	Albedo	%NArea	Cloud effect %NEAA	Weighted Albedo %
	A	*B*	*C* = *B* × (1–0.67)	*A* × *C*
Sum of water type		71		
Sea Ice	0.6	14.06	4.435	2.507
Water	0.06	56.94	18.995	1.14
Sum of land type		29	23.43	
Land - (UHI + Coverage)	0.312	28.941	9.551	2.978
UHI + Coverage	0.12	0.059	0.02	0.002
		100.000	33.000	6.64
			Cloud area	
Clouds	0.334	67	67	22.353
∑ Sum Earth %			123.430	
∑ Global Albedo				29.244

Here 15% is the total sea ice (see for example Table 5a) and 0.6 × 15% is sea ice percent in the Arctic area, 0.257 is the fraction of sea ice lost, and 40% is the solar irradiance effect. Then adding the Antarctic average sea ice area, the total sea ice area is reduced from 15% to

$$\text{Sea Ice area 2019} = 0.4 \times 15\% + 8.064 = 14.06\% \tag{36}$$

This is a 0.94% decrease from 15%. In the WAS model, we will have to assume that the effective ocean surface area increases proportionately by 0.94% to 56.94% (see Table 10). The WAS model then finds that the global albedo change decreases from 29.412 to 29.244%. (Note that alternately we could have set the albedo to 29.412% in 2019 and worked back to 1950. In this case, the albedo would have increased to 29.244%.)

The percent global warming (GW) is found as:

$$\%\mathrm{GW} = \left\{ (P/\sigma))^{0.25}_{2019} - (P/\sigma)^{0.25}_{1950} \right\} / 0.95\ ^{\circ}\mathrm{C}, \tag{37}$$

where $P = 340\ \mathrm{W/m^2} \times (1 - \mathrm{Albedo})$. The warming increase due to ice melting is estimated from this model to be about 0.15 °C or 15.8% when compared to a warming trend of 0.95 °C increase in 2019. The increase in radiative forcing is 0.6 $\mathrm{W/m^2}$. The feedback is then roughly 0.63 $\mathrm{W/m^2/°K}$ where we assume a temperature change of 0.95 °C.

These values should only be taken as a rough estimate due to numerous uncertainties as climatologists find it hard to fully quantify the seasonal variations in ice change and to know the possible impact on cloud coverage increase from additional warming evaporation. However, in the conclusion, this estimate is shown to help provide reasonable estimates related to GW assessments suggesting reasonable accuracy.

Appendix 5: WAASU model references

Table 11 provides references for the WAASU model values.

Table 11 Key references for WAASU model

Parameter	Albedo references	1950 area references
Sea Ice	50–70%, average 60% (NSID [54])	15% (Lindsey [55])
Water	6% (NSID [54])	56% Ocean + Sea Ice = 71% (USGS [56])
Land-(UHI + Coverage)	Adjusted to obtain 29.412% and surface reflected of 7.06 Earth Albedo in 1950 thereafter held fixed (see IPCC Hartmann [8] AR5 report)	29%-Urban Coverage
Avg. UHI + Cov	0.12 Sugawara et al. [48], 0.15 Tricia, A [38]	See Table 1
Clouds	22.353 (IPCC Hartmann et al. [8])	67% (Earthobservatory, NASA [37])
Earth Albedo	29.412% (IPCC Hartmann [8])	–

Appendix 6: Albedo model renormalization information

Table 12 is reproduced from above, while Table 13 shows the results of the Schneider dome area case. The results are used to demonstrate how normalization is performed

Normalization is done as follows:

1. The model starts with 1950 Table 12 albedo 29.412%, and then, the 2019 urban coverage area is entered.
2. For example, in Table 12, Column B the UHI area increases from **0.059%** to 1.143% (not shown) and normalized to **1.131**%. This value is 1.084% larger (= 1.143–0.059), now the “Sum of % of Earth Area” is increased from 100 to 101.084% in 2019.
3. All areas need to be renormalized to 101.084%. For example, sea ice at 15% in 1950 becomes 15% × (100.000/101.084) = **14.839%** and the urban coverage becomes 1.143% × (100/101.084) = 1**.1307%**.

We also include in this appendix the GRUMP dome estimates. Table 14 is reproduced from above, while Table 15 shows the results of the GRUMP dome area case.

Table 12 Schneider 1950 estimates

Surface	Albedo	%NEAA	Cloud effect %NEAA	Weighted Albedo %
	A	*B*	*C* = *B* × (1–0.67)	*A* × *C*
Sum of water type		71		
Sea ice	0.6	15	4.95	2.970
Water	0.06	56	18.48	1.109
Sum of land type		29		
Land - (UHI + Coverage)	0.312	28.941	9.551	2.978
UHI + Coverage	0.12	0.059	0.02	0.002
		∑ = 100.000	33.000	7.059
			Cloud area	
Clouds	0.334	67	67	22.353
∑ Sum Earth %			100.000	
∑ Global Albedo				29.412

Table 13 Schneider 2019 Dome estimate (AF = 8.4)

Surface	Albedo	%NEAA	Cloud effect %NEAA	Weighted Albedo %
	A	B	$C=B\times(1-0.67)$	$A\times C$
Sum of water type		70.239		
Sea ice	0.6	14.839	4.897	2.938
Water	0.06	55.4	18.282	1.097
Sum of land type		29.761		
Land - (UHI + Coverage)	0.312	28.631	9.448	2.946
UHI + Coverage	0.12	1.1307	0.373	0.045
		∑ = 100.000	33.000	6.981
			Cloud area	
Clouds	0.334	67	67	22.353
∑ Sum Earth %			100.000	
∑ Global Albedo				29.379

Table 14 GRUMP area 1950 estimates

Surface	Albedo	%NEAA	Cloud effect %NEAA	Weighted Albedo %
	A	B	$C=B\times(1-0.67)$	$A\times C$
Sum of water type		71		
Sea ice	0.6	15	4.95	2.970
Water	0.06	56	18.48	1.109
Sum of land type		29		
Land - (UHI + Coverage)	0.314	28.684	9.466	2.968
UHI + Coverage	0.12	0.316	0.104	0.013
		∑ = 100.000	33.000	*7.059*
			Cloud area	
Clouds	0.333	67	67	*22.353*
∑ Sum Earth %			100.000	
∑ Global Albedo				*29.412*

Table 15 GRUMP 2019 dome estimates (AF = 8.4)

Surface	Albedo	%NEAA	Cloud effect %NEAA	Weighted Albedo %
	A	B	$C=B\times(1-0.67)$	$A\times C$
Sum of water type		70.239		
Sea ice	0.6	14.239	4.7	2.82
Water	0.06	53.160	17.54	1.05
Sum of land type		29		
Land – (UHI + Coverage)	0.314	27.229	9.0	2.82
UHI + Coverage	0.12	5.371	1.77	0.21
		∑ = 100.000	33.000	6.9
			Cloud area	
Clouds	0.334	67	67	22.353
∑ Sum Earth %			100.000	
∑ Global Albedo				29.255

Appendix 7: Overview of estimates in Table 8

The GHG re-radiation effect increases the LWR forcing found in Table 7 by a factor of 1.62 as indicated in Table 4 (see also Feinberg [39]). Then, the LWR is modified using this by the standard formula

$$P_{2019} = 340\ \mathrm{W/m^2} \times (1 - \mathrm{Albedo}_{2019}) \times 1.62 \text{ and } P_{1950} = 340\ \mathrm{W/m^2} \times (1 - \mathrm{Albedo}_{1950}) \times 1.62 \tag{38}$$

Using this the UHI radiation forcing is

$$\Delta P = P_{2019} - P_{1950} \tag{39}$$

The results from this equation are shown in Table 8, Column 4 for each albedo. Next, we obtain a temperature increase. This is given by

$$\Delta T = \left\{ \left(P_\alpha/\sigma\right)^{0.25}_{2019} - \left(P_\alpha/\sigma\right)^{0.25}_{1950} \right\} \tag{40}$$

The results are shown in Table 8, Column 5.

Example In Table 8, the Schneider dome case having $0.182\ \mathrm{W/m^2}$ of forcing and $\Delta T_{\mathrm{rise}} = 0.034$ °C is illustrated.

The forcing (with the average re-radiation factor 1.62) is given as

$$\begin{aligned}\Delta P &= \left[340\ \mathrm{W/m^2} \times (1 - 0.29379)_{2019} \times 1.62\right] \\ &\quad - \left[340\ \mathrm{W/m^2} \times (1 - 0.29412)_{1950} \times 1.62\right] \\ &= 0.182\ \mathrm{W/m^2}\end{aligned} \tag{41}$$

and the temperature rise is

$$\begin{aligned}\Delta T = &\left(\left[\frac{1}{\sigma}340\ \mathrm{W/m^2} \times (1 - 0.29379) \times 1.62\right]^{0.25}\right)_{TS2019} \\ &- \left(\left[\frac{1}{\sigma}340\ \mathrm{W/m^2} \times (1 - 0.29412) \times 1.62\right]^{0.25}\right)_{TS1950} = 0.034\ ^\circ\mathrm{C}\end{aligned} \tag{42}$$

as indicated in Table 8.

IPCC/NOAA radiation forcing and percent global warming comparison

To make comparisons to assess the relative UHI forcing, the above results are referenced to the IPCC estimate for GHG forcing from the period 1950 to 2019, and this associated temperature rise. The GHG forcing estimate by IPCC/NOAA [41] for this period on GHG forcing is $2.38\ \mathrm{W/m^2}$.

One should note that this value does not include "feedback" (i.e., arctic snow and ice melting) as "forcing" is our primary concern. Column 6 then shows the relative forcing ratio to compare it to the UHI strength. For example, the LWR found in the Schneider case in Table 7 for the albedo of 29.3994 is $0.042\ \mathrm{W/m^2}$. Then, we estimate an average of $0.042\ \mathrm{W/m^2} \times 1.6 = 0.068\ \mathrm{W/m^2}$ for the full forcing using the GHG re-radiation factor of 1.62. Then relative to the IPCC GHG forcing estimate, this is about 2.9% (=0.068/2.38) shown in Table 8, Column 6.

IPCC/NOAA global temperature rise due to forcing comparison

Next, we estimate the percent of global warming anticipated from the WAASU model results. To do this we need an estimate of the temperature rise due to IPCC/NOAA [41] GHG forcing assessment to make comparisons. Using the albedo of 29.412 for 1950 (Table 7), then the LWR GHG re-radiation energy (using the 1.62 Factor) is

$$P_{\alpha 1950} = 340\ \mathrm{W/m^2} \times (1 - .294118) \times 1.62 = 388.8\ \mathrm{W/m^2} \tag{43}$$

This is converted to the 1950 temperature providing a reasonable estimate of the average global temperature for that year

$$T_{1950} = \left(388.8\ \mathrm{W/m^2}/\sigma\right)^{0.25} = 387.76\ ^\circ\mathrm{K}\ (14.61\ ^\circ\mathrm{C}) \tag{44}$$

Then, the forcing (without feedback) for 2019 according to the IPCC/NOAA [41] value of 2.38 W/m2 yields a total radiation of

$$P_{F\alpha 2019} = 388.8\ \mathrm{W/m^2} + 2.38\ \mathrm{W/m^2} = 388.2\ \mathrm{W/m^2} \tag{45}$$

This converts to the following temperature

$$T_{F\_2019} = \left(391.2\ \mathrm{W/m^2}/\sigma\right)^{0.25} = 288.2\ ^\circ\mathrm{K}(15.048\ ^\circ\mathrm{C}) \tag{46}$$

This provides a temperature rise of 0.44 °C

$$\Delta T_{\mathrm{Forcing}} = T_{F\_2019} - T_{1950} = 15.048\ ^\circ\mathrm{C} - 14.609\ ^\circ\mathrm{C} = 0.44\ ^\circ\mathrm{C} \tag{47}$$

We note the actual temperature rise with feedback is 0.95 °C in 2019. This would require a feedback factor of about 2.15. The factor of 2 has been cited in the literature [27–29], so this is a reasonable estimate. If we consider this to be the actual temperature rise due to all forcing (taken from the IPCC GHG estimate), the relative global warming contribution from the UHI temperature rise is shown in Table 8 in the last column. This is the same as the ratio of GHG forcing. For example, ΔT is 0.013 °C for the albedo decrease from 29.4418 to 29.3994% from Eqs. 13–15. Then, the percent of global warming relative to 0.44 °C is 2.9% (=0.013C/0.44C percent).

Finally, examples for Eq. 15 and 16 are provided below:

Example for Eq. 15: Eq. 15 can be used for reverse forcing. From Equation 15, the global albedo change required for IPCC/NOAA forcing estimate of 2.38W/m^2 requires a −1.47% change equal to a global albedo increase of 0.0043 for reverese forcing. As another example, given a global albedo change by 0.2% the forcing expected is

$$\alpha_{\mathrm{Global\_Forcing}} = 1.6\,2 \times\ 1\ \mathrm{W/m^2}\%\Delta_{\mathrm{albedo}} \times 0.2\% = 0.32\,\mathrm{W/m^2}\ (\text{Table 8, Row 4}) \tag{48}$$

Example for Eq. 16: Given a UHI EAA of 1.14% then the forcing is

$$\mathrm{UHI}_{\mathrm{EAA\_Forcing}} = 1.62\ \times\ 0.096\ \mathrm{W/m^2}\%\mathrm{EAA} \times\ 1.14\% = 0.18\ \mathrm{W/m^2}\left(\text{Table 8, Row 3, } 0.18\ \mathrm{W/m^2}\right) \tag{49}$$

References

1. McKitrick R, Michaels J (2004) A test of corrections for extraneous signals in gridded surface temperature data. Clim Res 26:159–173
2. McKitrick R, Michaels P (2007) Quantifying the influence of anthropogenic surface processes and inhomogeneities on gridded global climate data. J Geophys Res Atmos. Also see McKitrick Website Describing controversy: https://www.rossmckitrick.com/temperature-data-quality.html. Accessed 1 Nov 2020
3. De Laat ATJ, Maurellis AN (2006) Evidence for the influence of anthropogenic surface processes on lower tropospheric and surface temperature trends. Int J Climatol 26:897–913
4. IPCC Archive (2007) https://archive.ipcc.ch/publications_and_data/ar4/wg1/en/ch3s3-2-2-2.html. Accessed 1 Nov 2020
5. Schmidt GA (2009) Spurious correlations between recent warming and indices of local economic activity. Int J Climatol A J Roy Meteorol Soc 29:2041–2048
6. McKitrick R (2010) Atmospheric oscillations do not explain the temperature-industrialization correlation. Stat Politics Policy 1(1)
7. McKitrick R, Nierenberg N (2010) Socioeconomic patterns in climate data. J Econ Soc Meas 35(3,4):149–175. https://doi.org/10.3233/jem-2010-0336
8. Hartmann DL, Klein Tank AMG, Rusticucci M, Alexander LV, Brönnimann S, Charabi Y, Dentener FJ, Dlugokencky EJ, Easterling DR, Kaplan A, Soden BJ, Thorne PW, Wild M, Zhai PM (2013) Observations: atmosphere and surface. In: Climate change (2013) the physical science basis. Contribution of working group I to the fifth assessment report of the intergovernmental panel on climate change. Cambridge University Press, Cambridge, United Kingdom and New York, NY, USA
9. Zhao Z-C (1991) Temperature change in China for the last 39 years and urban effects. Meteorol Mon 17(4):14–17 **(in Chinese)**
10. Feddema JJ, Oleson KW, Bonan GB, Mearns LO, Buja LE, Meehl GA, Washington WM (2005) The importance of land-cover change in simulating future climates. Science 310:1674–1678. https://doi.org/10.1126/science.1118160
11. Ren G-Y, Chu Z-Y, Zhou J-X et al (2008) Urbanization effects on observed surface air temperature in North China. J Clim 21:1333–1348
12. Jones PD, Lister DH, Li Q-X (2008) Urbanization effects in large-scale temperature records, with an emphasis on China. J Geophys Res 113:D16122. https://doi.org/10.1029/2008jd009916
13. Stone B (2009) Land use as climate change mitigation. Environ Sci Technol 43(24):9052–9056. https://doi.org/10.1021/es902150g
14. Zhao Z-C (2011) Impacts of urbanization on climate change. Earth Science, Science Press, New York, pp 843–846
15. Yang X, Hou Y, Chen B (2011) Observed surface warming induced by urbanization in east China. J Geophys Res Atmos. https://doi.org/10.1029/2010jd015452
16. Huang Q, Lu Y (2015) Effect of Urban heat island on climate warming in the Yangtze river Delta Urban agglomeration in China. Int J Environ Res Public Health 12(8):8773
17. Bian T, Ren G, Yue Y (2017) Effect of urbanization on land-surface temperature at an urban climate station in north China. Bound Layer Meteorol 165:553–567
18. Conference of the Parties, Adoption of the Paris Agreement (2015) U.N. Doc. FCCC/CP/2015/L.9/Rev/1
19. Satterthwaite DE, Aragón-Durand F, Corfee-Morlot J, Kiunsi RBR, Pelling M, Roberts DC, Solecki W (2014) Urban areas. In: Climate change impacts, adaptation, and vulnerability. Part A: global and sectoral aspects. Contribution of working group II to the fifth assessment report of the intergovernmental panel on climate change (IPCC)
20. Schneider A, Friedl M, Potere D (2009) A new map of global urban extent from MODIS satellite data. Environ Res Lett 4(4):044003. https://doi.org/10.1088/1748-9326/4/4/044003
21. Global Rural Urban Mapping Project (GRUMP) (2005) Columbia university socioeconomic data and applications center, gridded population of the world and the global rural-urban mapping project (GRUMP)
22. NASA (2000) Gridded population of the world. https://sedac.ciesin.columbia.edu/data/set/gpw-v3-population-count/data-download. Accessed 1 Mar 2020
23. Galka M (2016) Half the world lives on 1% of its land, mapped. https://www.citylab.com/equity/2016/01/half-earth-world-population-land-map/422748/, (2016 publication on 2000 data set) http://metrocosm.com/world-population-split-in-half-map/. Accessed 1 Mar 2020
24. Zhou Y, Smith S, Zhao K, Imhoff M, Thomson A, Lamberty B, Asrar G, Zhang X, He C, Elvidge C (2015) A global map of urban extent from nightlights. Environ Res Lett 10 (2000 data set)
25. Karl TR, Diaz HF, Kukla G (1988) Urbanization: its detection and effect in the United States climate record. J Clim 1:1099–1123
26. Chagnon SA (1999) A rare long record of deep soil temperature defines temporal temperature changes and an urban heat island. Clim Change 42:531–538
27. Manabe S, Wetherald RT (1967) Thermal equilibrium of the atmosphere with a given distribution of relative humidity. J Atmos Sci 24:241–259
28. Randall DA et al (2007) Climate models and their evaluation. In: Solomon S et al (eds) Climate change 2007: the physical science basis. Contributions of working group I to the fourth assessment report of the intergovernmental panel on climate change. Cambridge Univ. Press, Cambridge

29. Dessler AE, Zhang Z, Yang P (2008) Water-vapor climate feedback inferred from climate fluctuations, 2003–2008. Geophys Res Lett. https://doi.org/10.1029/2008GL035333
30. Zhang X, Friedl MA, Schaaf CB, Strahler AH, Schneider A (2004) The footprint of urban climates on vegetation phenology. Geophys Res Lett 31:L12209
31. Zhou D, Zhao S, Zhang L, Sun G, Liu Y (2015) The footprint of urban heat island effect in China. Sci Rep 5:11160
32. Fan Y, Li Y, Bejan A et al (2017) Horizontal extent of the urban heat dome flow. Sci Rep 7:11681. https://doi.org/10.1038/s41598-017-09917-4
33. World Bank (2018) population growth rate. www.worldbank.org. Accessed 1 Mar 2020
34. USGS (1900-2006) Materials in use in U.S. interstate highways. https://pubs.usgs.gov/fs/2006/3127/2006-3127.pdf. Accessed 1 Mar 2020
35. US Population Growth (1900–2006). u-s-history.com/pages/h980.html. Accessed 1 Mar 2020
36. NASA (2020) https://climate.nasa.gov/vital-signs/global-temperature/. Accessed 1 Mar 2020
37. Earthobservatory, NASA (clouds albedo 0.67) https://earthobservatory.nasa.gov/images/85843/cloudy-earth. Accessed 1 Mar 2020
38. Tricia A, Hutyra L, Schaaf C, Erb A, Wang J (2017) Albedo, land cover, and daytime surface temperature variation across and urbanized lanscape. AGU. https://doi.org/10.1002/2017EF000569
39. Feinberg A (2020) On geoengineering and implementing an albedo solution with UHI GW and cooling estimates vixra 2006.0198. https://doi.org/10.13140/rg.2.2.26006.37444/6 (Currently in Peer Review in the J Mitig Adapt Strat Glob Change)
40. He T, Liang S, Song DX (2014) Analysis of global land surface albedo climatology and spatial-temporal variation during 1981–2010 from multiple satellite products. J Geophys Res Atmos 119:10281–10298. https://doi.org/10.1002/2014JD021667
41. Butler J, Montzka S (2020) The NOAA annual greenhouse gas index, earth system research lab. Global Monitoring Laboratory. https://www.esrl.noaa.gov/gmd/aggi/aggi.html. Accessed 5 Aug 2020
42. Liu Z, He C, Zhou Y et al (2014) How much of the world's land has been urbanized, really? A hierarchical framework for avoiding confusion. Landsc Ecol 29:763–771. https://doi.org/10.1007/s10980-014-0034-y
43. Cao C, Zhao J, Gong P, Ma G, Bao D, Tian K (2011) Wetland changes and droughts in southwestern China. Geomat Natural Hazards Risk. https://doi.org/10.1080/19475705.2011.588253
44. Zhao L, Lee X, Smith R, Oleson K (2014) Strong, contributions of local background climate to urban heat islands. Nature 10:511(7508):216–219. https://doi.org/10.1038/nature13462
45. Gunawardenaa K, Wells M, Kershawa T (2017) Utilising green and blue space to mitigate urban heat island intensity. ScienceDirect. https://doi.org/10.1016/j.scitotenv.2017.01.158
46. Akbari, H, Matthews HD, Seto D (2012) The long-term effect of increasing the albedo of urban areas. Environ Res Lett **7**(2):159–167. https://doi.org/10.1088/1748-9326/7/2/024004. Bibcode:2012ERL7b4004A
47. Connor Steve (2012) Painting roofs white is as green as taking cars off the roads for 50 years, says study. The Independent, London
48. Sugawara H, Takamura T (2014) Surface albedo in cities (0.12): case study in Sapporo and Tokyo, Japan. Bound Layer Meteorol 153:539–553. https://doi.org/10.1007/s10546-014-9952-0
49. Basara J, Hall Jr P, Schroeder A, Illston B, Nemunaitis K (2008) Diurnal cycle of the Oklahoma City urban heat island. J Geophys Res
50. Barr JM (2019) The economics of skyscraper height (part IV): construction costs around the world. https://buildingtheskyline.org/skyscraper-height-iv/. Accessed 1 Apr 2020
51. NOAA, Scott M (2019) Understanding climate: Antarctic sea ice extent. https://www.climate.gov/print/833949. Accessed 1 Apr 2020
52. NASA Sea Ice (2019) https://climate.nasa.gov/vital-signs/arctic-sea-ice/. Accessed 1 Apr 2020
53. Sciencing (2018) https://sciencing.com/sun-intensity-vs-angle-23529.html. Accessed 1 Apr 2020
54. NSID (2020) National snow and ice data center. Thermodynamics: Albedo. nsidc.org. Retrieved 14 August 2016. https://nsidc.org/cryosphere/seaice/processes/albedo.html. Accessed 1 Mar 2020
55. Lindsey R, Scott M (2019) Climate change: Arctic sea ice summer minimum, NOAA Climate.gov. https://www.climate.gov/news-features/understanding-climate/climate-change-minimum-arctic-sea-ice-extent. Accessed 1 Mar 2020
56. USGS on Amount of Earth covered by water. https://www.usgs.gov/special-topic/water-science-school/science/how-much-water-there-earth?qt-science_center_objects=0#qt-science_center_objects. Accessed 1 Mar 2020